Donor–Acceptor Nanohybrids

DOI: 10.1002/ange.201207006

Self-Ordering Electron Donor–Acceptor Nanohybrids Based on Single-Walled Carbon Nanotubes Across Different Scales**

Fulvio G. Brunetti, Carlos Romero-Nieto, Javier López-Andarias, Carmen Atienza, Juan Luis López, Dirk M. Guldi, and Nazario Martín**

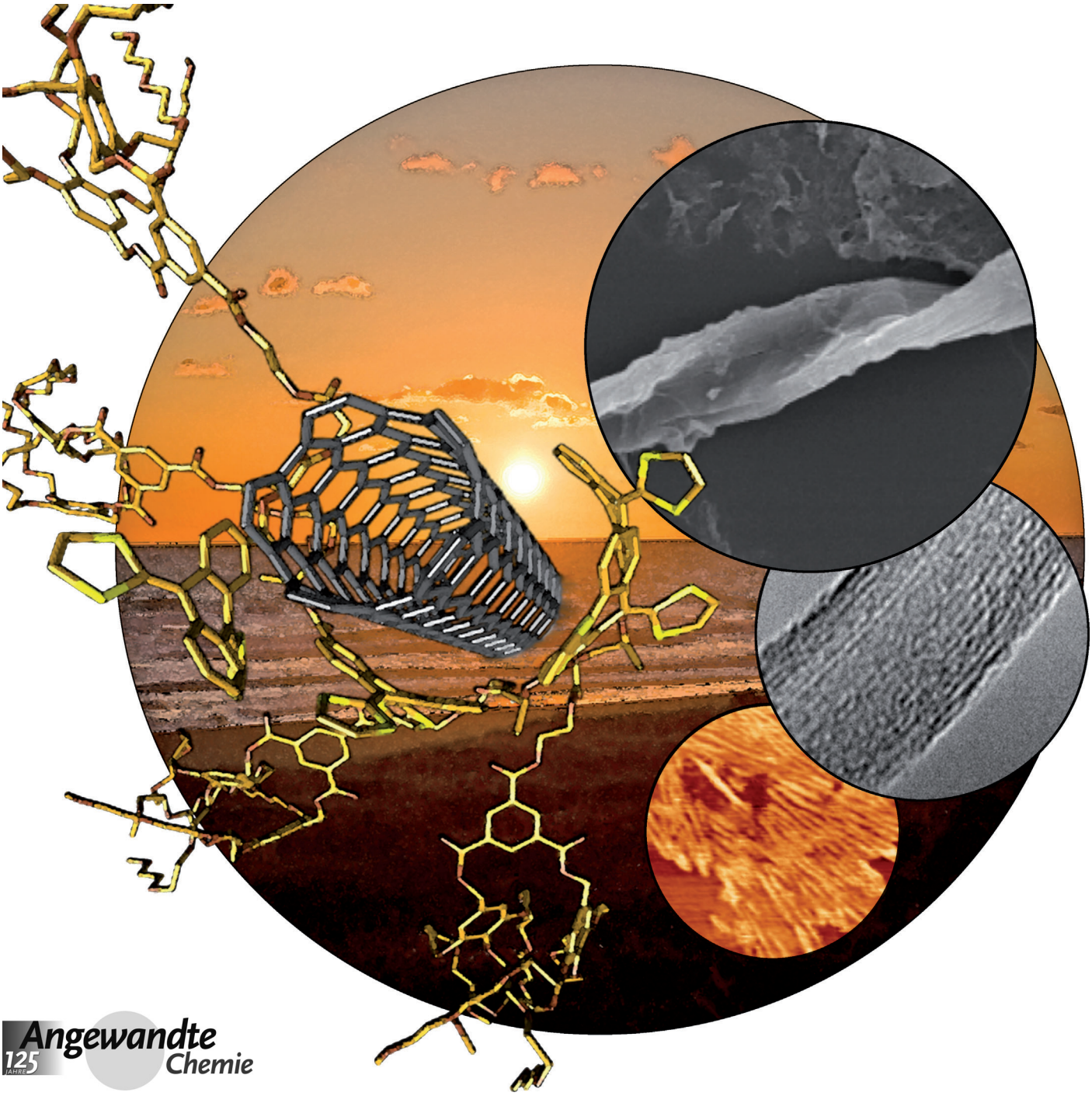

Control over self-assembling nanostructures constitutes a major challenge in contemporary research. As a reflection of the latter, a great deal of time and effort has gone into understanding the factors and parameters that govern the shape, size, and composition of nanostructures.[1]

An intriguing class of materials is carbon nanotubes (CNTs). CNTs have attracted considerable attention owing to their outstanding features, especially in electronics, mechanics, and optics. In fact, they are found in applications that range from drug delivery to organic electronics.[2] Soon after the discovery of multi-walled carbon nanotubes (MWCNTs) in 1991 by Iijima, single-walled carbon nanotubes (SWCNTs) were independently reported by Iijima and Bethune in 1993.[3] Conceptionally, SWCNTs are thought of as one-dimensionally extended fullerenes, in which the sidewalls are composed of rolled up graphene sheets and the caps are made out of hemispherical fullerenes.[4]

When dealing with SWCNTs, limited control over their growth and homogeneous production imposes, however, major drawbacks for emerging areas of nanotechnology. Equally problematic is their rather poor solubility in common organic solvents. Large spaghetti-like bundles, that originate from attractive interactions such as π–π stacking and London dispersion forces, are the cause of insolubility.[5] In fact, the latter renders purification, separation, and manipulation of SWCNTs a sheer impossible task.[6]

To exploit the full potential of SWCNTs and to overcome any of the aforementioned limitations, their covalent and noncovalent chemistry has developed into a rather valuable and mature field.[7] For example, functional groups have covalently been added to the sidewalls and caps of SWCNTs by means of versatile synthetic protocols. In such cases, the electronic structure of the SWCNTs is irreversibly altered and, in turn, the overall π-systems reveal notable perturbation. Contrarily, noncovalent functionalization of SWCNTs has mostly been based on fairly weak π–π and/or hydrogen-bonding interactions. In the resulting nanohybrids, SWCNTs are coated/wrapped, and, thus, intertube interactions are minimized, whereas the intrinsic electronic properties are preserved.[8] To date, the noncovalent strategy en route towards multifunctional systems is the method of choice to fully harvest the unique features of SWCNTs in, for example, p-/n-type electron donor–acceptor nanohybrids.[9]

Usually, p-/n-type electron donor–acceptor nanohybrids based on SWCNTs have been obtained by employing conjugated materials that lack the means to control the morphology.[10] On the contrary, polypeptides,[11] polysaccharides,[12] DNA strains,[13] and foldable oligomers[14] have extensively been used to form ordered SWCNT nanohybrids, albeit they fail to feature the electron-donating ability and, in turn, appreciable electronic communication.

Here, we have designed a photo- and redox-active 9,10-di(1,3-dithiol-2-ylidene)-9,10-dihydroanthracene (exTTF) covalently linked to an alanyl-glycine dipeptide sequence bearing a polyethylene glycol dendrimer (Scheme 1). Our straightforward design enables supramolecular organization across scales, that is, from the nano- to the macroscale, and probing the photophysical properties of the resulting electron donor–acceptor nanohybrids. In fact, we will demonstrate that exTTF-based dipeptide **1** guarantees the noncovalent functionalization of SWCNTs affording unique p-/n-type nanohybrids, the generation of long-lived radical ion pairs, and the introduction of SWCNT nanostructuring at the nanoscale amalgamating into macroscale domains of aligned SWCNTs, especially in polar and aqueous media.

The retrosynthetic analysis for **1** is illustrated in Scheme 1. **1** was obtained by linking building blocks **2**,[15] **3**, and **4** (see

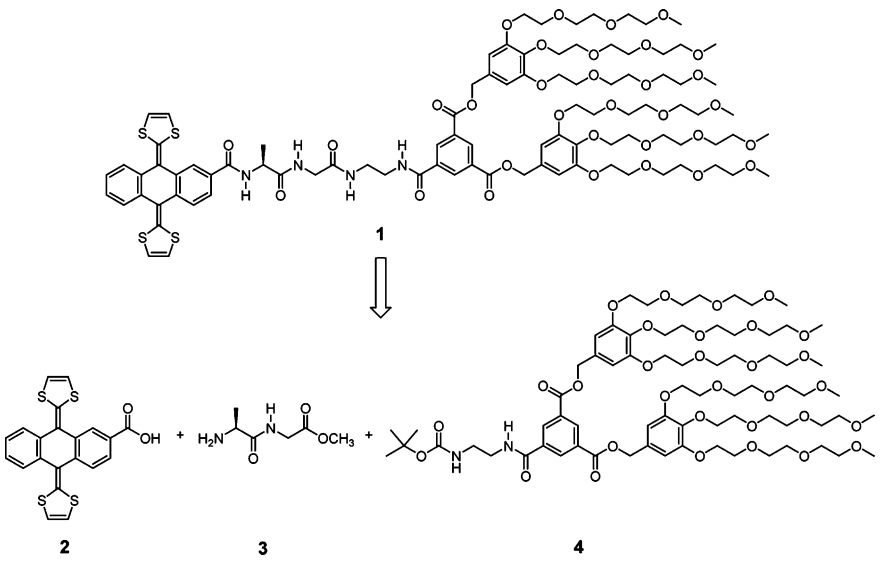

Scheme 1. Retrosynthetic scheme of the π-extended tetrathiafulvalene **1**.

[*] Dr. F. G. Brunetti, J. López-Andarias, Dr. C. Atienza, Dr. J. L. López, Prof. N. Martín
Departamento de Química Orgánica, Facultad de C.C. Químicas
Ciudad Universitaria sn (Spain)
and
IMDEA-nanociencia, 28049, Madrid (Spain)
E-mail: nazmar@quim.ucm.es
Homepage: http://www.ucm.es/info/fullerene
Dr. C. Romero-Nieto, Prof. D. M. Guldi
Department of Chemistry and Pharmacy & Interdisciplinary Center for Molecular Materials
University of Erlangen-Nuremberg
Egerlandstr. 3, 91058 Erlangen (Germany)

[**] Financial support by the Ministerio de Ciencia e Innovación (MINECO) of Spain (projects CTQ2011-24652 and Consolider-Ingenio CSD2007-00010), the EU (FUNMOLS FP7-212942-1) the CAM (MADRISOLAR-2 project S2009/PPQ-1533) is acknowledged. We also thank to the Deutsche Forschungsgemeinschaft (SFB583), the Office of Basic Energy Sciences of the U.S., and Solar Technologies Go Hybrid. The MINECO of Spain is thanked by C.A. for a Ramón y Cajal contract.

Supporting information for this article is available on the WWW under http://dx.doi.org/10.1002/anie.201207006.

the Supporting Information). Initially, **2** and **3** were coupled by amidation in the presence of activating agents. Deprotection of the methyl esthers and subsequent reaction with deprotected **4** led to the formation of target **1** in excellent yields.

1/SWCNT nanohybrids were obtained following an already established protocol without, however, the needs of employing any surfactants (see the Supporting Information).[16] Upon their formation, **1**/SWCNTs were fully characterized by means of TEM, SEM, AFM, small angle X-ray scattering (SAXS), absorption, and Raman spectroscopy.

For **1**/SWCNTs, representative TEM images are displayed in Figure 1 a,b and Figure S1. At first glance, a high degree of nanohybrid organization is discernable. A closer look reveals the formation of fairly well-aligned SWCNT structures (Figure 1 b,c). The latter agrees well with a report by Dieckman et al., who have reported that with the help of a polypeptide (i.e., 29 amino acids lacking an electron donor) aligned water-soluble SWCNTs were obtained.[11] In stark contrast to their case, we have focused on aligning SWCNTs with a water-soluble dipeptide sequence bearing dendrimeric and electron-donating termini. When compared to pristine SWCNTs, **1**/SWCNTs lack any randomly aggregated bundles. SWCNTs reveal, for instance, bundles with diameters that range from 12 to 50 nm (Figure S1b).

In control experiments, dichloromethane, which was used instead of water, gave an organization that is best described as the coexistence of **1**, unfunctionalized, pristine SWCNTs, and **1**/SWCNTs (Figure 1 d). The different organization relates to the rather strong change in solvent polarity, that is, water versus dichloromethane. Well-aligned SWCNTs have only been seen in experiments with chemical vapor deposition techniques.[17] In such a specific protocol SWCNTs are forced to align in parallel.

SEM analysis further confirmed self-aligning **1**/SWCNTs and a clear higher organization of these nanocomposites is discerned in Figure 2. Particularly, Figure 2 b shows a magnification of the self-oriented SWCNTs and their ordered structure.

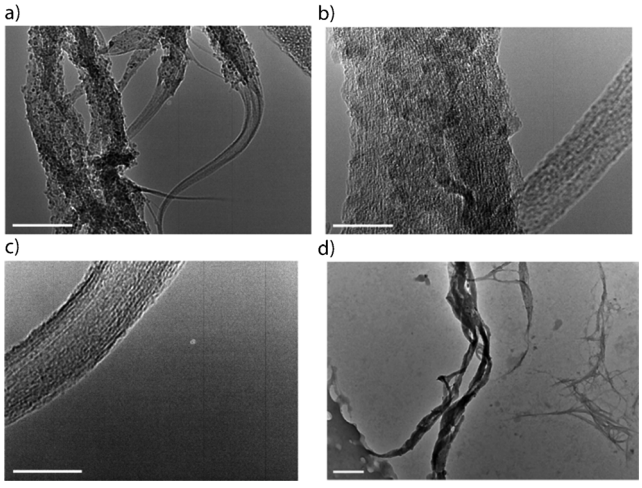

Figure 1. a–c) TEM images of **1**/SWCNTs drop-coated from water at different magnifications—scale bars of 100, 20, and 20 nm, respectively. d) TEM image of **1**/SWCNTs drop-coated from DCM—scale bar of 200 nm.

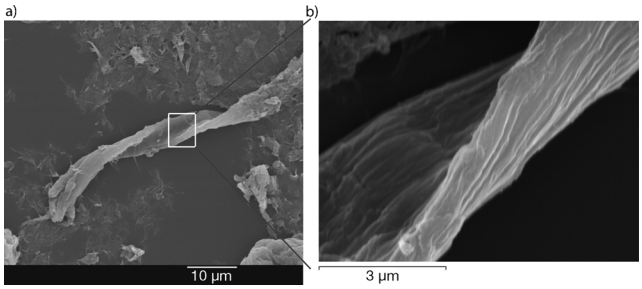

Figure 2. SEM images of coated **1**/SWCNTs (left) and an amplification of the self-organization of SWCNT hybrids (right).

Likewise, our AFM assays prompt to the formation of 2D organized domains that are exclusively composed of **1**/SWCNTs. On highly ordered pyrolytic graphite (HOPG) wafers, AFM images reveal upon correcting for the tip-broadening, a lateral *d*-spacing for the 2D nanocomposite of around 10 nm. (See the Materials and Methods Section in the Supporting Information.) FFT analyses of the AFM images point unmistakably towards the preferred SWCNT alignment in the resulting 2D order (Figure 3 a). Height profiles underscore that **1**/SWCNTs posses heights in excess of 2.5 nm (Figure 3 c).

Histograms, in which the AFM diameter distributions of **1**/SWCNTs are gathered, are displayed in Figure 3 d. These imply the homogeneous immobilization of **1** onto individualized SWCNTs. Accordingly, we derive from AFM that more than 80 % of the nanostructures are formed by individual **1**/SWCNTs laterally assembled into two dimensions (Figure 3 b).

In solution, the presence of well-ordered **1**/SWCNTs was confirmed by means of SAXS measurements. X-ray scattering of **1**/SWCNTs in aqueous media at 25 °C gives rise to a q^{-4} dependence within the low "q" range, which is indicative for the presence of large aggregates. In addition, a scattering peak in the intermediate "q" range with a spacing of approximately 8.97 nm is discernible (Figure 3 e). Please note that this spacing is in excellent agreement with the lateral *d*-spacing observed after the tip-broadening correction in AFM. On one hand, such spacing is in the range of **1**/SWCNT diameters (Figure 3 f). On the other hand, such spacing suggests that an effective shielding/coating of **1** leads to the individualization of SWCNTs and results from a uniform and homogeneous SWCNT functionalization. Important are also the hydrophilic dendrimer termini, which favor engagement with the surrounding water (Figure 3 f). SAXS measurements with just **1** as control lack any ordered supramolecular ensemble in this media (Figure S3).

The results of our noncovalent functionalization strategy were further investigated by Raman spectroscopy, that is, the radial breathing mode (RBM) and D, G, and G′ modes. It should be mentioned upfront that the D band intensities in the Raman spectra of pristine SWCNTs and of **1**/SWCNTs reveal no difference. Such a similarity corroborates the absence of oxidative/damaging processes during the workup procedure. As a matter of fact, we hypothesize that the original SWCNT properties must be preserved in **1**/SWCNTs. What did change, however, were the RBM and D′ modes.

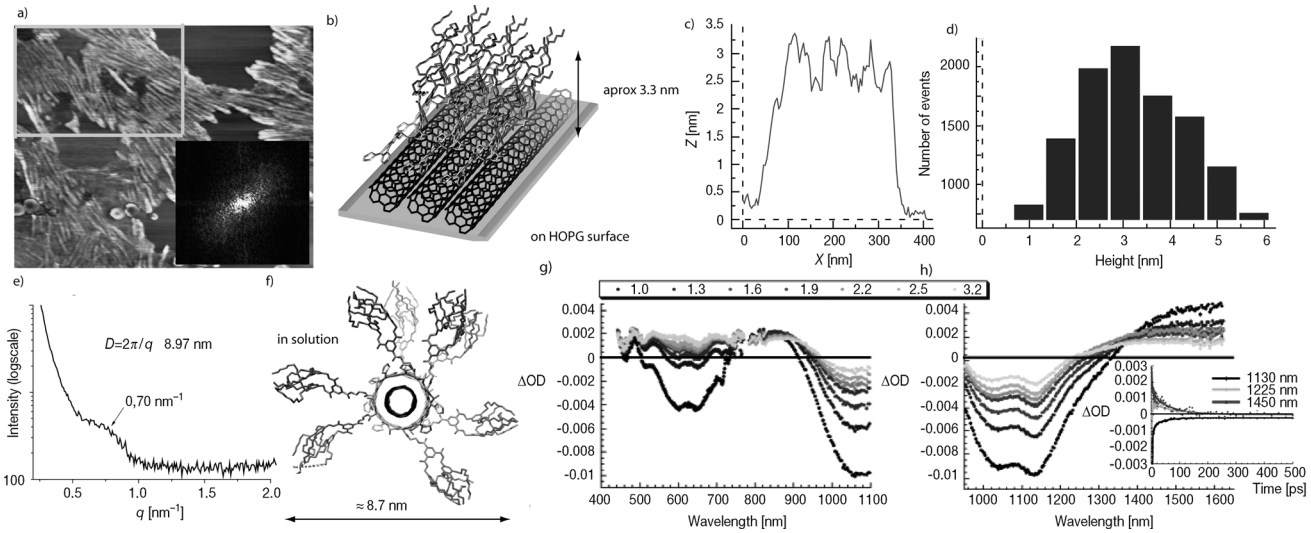

Figure 3. a) AFM images of **1**/SWCNTs on a HOPG surfaces (1 μm×1 μm). Inset: FFT analysis of the highlighted area in the square. b) Schematic drawing of **1**/SWCNTs on a HOPG surface. c) Height profile of the section highlighted in (a). d) Histogram of the height distribution. e) SAXS scattering of **1**/SWCNTs in aqueous solution at 25 °C. f) Schematic drawing of **1**/SWCNTs in solution. g and h) Differential absorption spectra obtained upon femtosecond pump–probe experiments (387 nm) of **1**/SWCNT in D_2O with several time delays between 1.0 and 13.0 ps at room temperature and in the visible/near-infrared and extended near-infrared regions, respectively. Inset h) Time absorption profiles at 1130, 1225, and 1450 nm monitoring the electron transfer.

They changed in intensity and frequency with an overall decrease and a 3.5 cm^{-1} shift to higher frequencies (Figure S2) revealing the needs of higher activation energies. RBMs are strictly related to SWCNT diameters, chiralities, and the presence of bundles.[18] Thus, modified RBMs are in agreement with data reported for wrapped SWCNTs.[19] Only in cases of high molecular weight macromolecules, which thoroughly wrap around SWCNTs, Raman shifts emerged that are as high as 3–5 cm^{-1}.[13] Commonly, no appreciable changes in the RBMs are detected for noncovalent interactions based on π–π interacting building blocks.[20]

Owing to the electron-donating and chromophoric features of the exTTFs, spectroscopic measurements were performed. To this end, we monitored the absorption of **1** in water and in the presence of increasing amounts of SWCNTs (Figure S4). Interestingly, the addition of SWCNTs resulted in an intensity decrease of the exTTFs centered features in the visible (i.e., 453 and 382 nm), the simultaneous increase of SWCNT absorptions in the near-infrared (i.e., vide infra), and the formation of pseudo-isosbestic and isobestic points at 363 and 489 nm, respectively. Further insights into the formation of **1**/SWCNTs came from variable temperature absorption analyses (Figure S5). Here, the absorption intensity of **1** increased as the temperature was raised up from RT to 90 °C without the formation of SWCNT precipitates (Figure S6). More importantly, the initial spectrum was recovered when the temperature was adjusted to the initial value. The aforementioned is in sound agreement with SWCNT debundling in water, especially at higher temperatures.[21] In addition, we monitored the absorption features of SWCNTs in the absence and presence of **1**. The addition of **1** to aqueous suspensions of SWCNTs evoked an appreciable red-shift of the absorption maxima from 570, 590, 653, 727, 985, 1023, and 1123 nm for sodium dodecylbenzene sulfonate (SDBS)/SWCNT to 576, 601, 661, 737, 1011, 1052, and 1157 nm for **1**/SWCNT (Figure S7). But it is not only the absorption features that are impacted by **1**, also the SWCNT fluorescence maxima shift bathochromically from 965, 1032, 1127, and 1256 nm for SDBS/SWCNT to 995, 1059, 1158, and 1296 nm for **1**/SWCNT. Interestingly, an overall fluorescence quenching of 91 % goes hand in hand with the formation of **1**/SWCNTs and, as such, prompts to a fast deactivation of photoexcited SWCNTs in the presence of **1** (Figures S8 and S9).

To shed light onto the fast excited-state deactivation in **1**/SWCNT, transient absorption measurements were performed.[22] Following laser excitation at 387 nm, SDBS/SWCNT gives rise to the instantaneous formation of a transient spectrum that features minima at 512, 597, 647, 1022, and 1131 nm, as well as maxima at 485 and 1430 nm. The SWCNT centered transient is metastable and its decay is dominated by two major processes. In fact, lifetimes of 2.8 and 67 ps result from a multiexponential decay of the aforementioned features. Owing to the shifts seen in the absorption spectra, photoexcitation of **1**/SWCNT at 387 nm leads to transient features that are red-shifted with respect to SDBS/SWCNT. For **1**/SWCNT, minima emerge at 462, 515, 601, 651, 1062, and 1155 nm, together with maxima at 485, 853 and 1492 nm. Figure 3 g,h shows that these features transform with a lifetime of 6 ps into a new transient. Importantly, the newly developing transient is composed in the visible range of a broad maximum at 685 nm. The latter resemble the one-electron oxidized radical cation of **1**. In the near-infrared, minima at 1014 and 1131 nm as well as maxima at 485, 535, 616, 883, and 1415 nm imply new conduction band electrons in SWCNTs. In other words, upon photoexcitation of **1**/SWCNT the singlet excited state gives rise to an electron transfer product, in which **1** is oxidized and SWCNTs are reduced. From multiwavelength analyses of the charge-separated state, we deduce a lifetime of 280 ± 20 ps, which is considerably longer than

that for a pyrene derivative functionalized with 9,10-di(1,3-dithiol-2-ylidene)-9,10-dihydroanthracene (π-extended tetrathiafulvalene)/SWCNT.[20]

To probe the electron-transfer impact of **1** on different SWCNTs, we turned to (6,5) and (7,6) enriched SWCNTs (Figures S11 and S12, respectively). Because of the SWCNT enrichment fewer minima, that is, at 475, 515, 665, 1055, and 1150 nm, evolve for **1**/(7,6) than for the mixture of **1**/SWCNT. In line with the size quantization the corresponding minima for **1**/(6,5) are blue-shifted to 475, 595, and 675 nm in the visible and to 1020 nm in the near-infrared when compared to **1**/(7,6). In both cases, charge separation leads within 5.0 ps to the oxidation of **1** with its prominent feature at 685 nm. Evidence for the SWCNT reduction, on the other hand, differs between **1**/(7,6) and **1**/(6,5) with minima at 1025/1140 and 1000 nm, respectively. Quite interesting is the trend seen in the charge recombination dynamics with 260 ± 10 ps for **1**/(6,5) and 105 ± 20 ps for **1**/(7,6). In other words, the lower charge-separated state energy in (6,5) SWCNTs is beneficial to stabilize the charge-separated state. From a comparison of the spectral changes we conclude that **1**/SWCNTs contain predominantly **1**/(7,6). On the contrary, comparing the charge recombination dynamics it appears that the dynamics in **1**/SWCNTs are governed predominantly by **1**/(6,5).

In summary, we have described a versatile noncovalent functionalization of SWCNTs in water. Our protocol enables the spontaneous self-assembly of SWCNTs into well-ordered structures of different scales. As such **1**/SWCNTs represent a unique example of short- and long-range organization induced by a short peptide sequence linked to electron-donating exTTF. Importantly, photoexcitation of **1**/SWCNTs affords SWCNT-centered excited states that transform into long-lived charge-separated states in water. Their stability is enhanced by long-range order. Likewise, self-ordering p-/n-type composites on the nano- and mesoscale are a rational and practical approach to the control of the morphology in a variety of electronic devices, the efficiency of which is decisively impacted by the molecular order and/or phase segregation.

Received: August 29, 2012
Revised: December 21, 2012
Published online: January 22, 2013

Keywords: carbon nanotubes · charge separation · donor–acceptor nanohybrids · self-assembly · spectroscopy

[1] a) S. S. Babu, S. Prasanthkumar, A. Ajayaghosh, *Angew. Chem.* **2012**, *124*, 1800 – 1810; *Angew. Chem. Int. Ed.* **2012**, *51*, 1766 – 1776; b) T. Aida, E. W. Meijer, S. I. Stupp, *Science* **2012**, *335*, 813 – 817; c) S. Yagai, M. Usui, T. Seki, H. Murayama, Y. Kikkawa, S. Uemura, T. Karatsu, A. Kitamura, A. Asano, S. Seki, *J. Am. Chem. Soc.* **2012**, *134*, 7983 – 7994.

[2] a) V. Sgobba, D. M. Guldi, *Chem. Soc. Rev.* **2009**, *38*, 165 – 184; b) *Carbon Nanotubes and Related Structures* (Eds.: D. Guldi, N. Martín), Wiley-VCH, Weinheim, **2010**; c) *Supramolecular Chemistry of Fullerenes and Carbon Nanotubes* (Eds.: N. Martin, J.-F. Nierengarten), Wiley-VCH, Weinheim, **2011**, chap. 10 – 12.

[3] a) S. Iijima, *Nature* **1991**, *354*, 56 – 58; b) S. Iijima, T. Ichihashi, *Nature* **1993**, *363*, 603 – 605; c) D. S. Bethune, C. H. Klang, M. S. de Vries, G. Gorman, R. Savoy, J. Vazquez, R. Beyers, *Nature* **1993**, *363*, 605 – 607.

[4] a) R. Saito, M. Fujita, G. Dresselhaus, M. S. Dresselhaus, *Appl. Phys. Lett.* **1992**, *60*, 2204 – 2206; b) J. L. Delgado, M. A. Herranz, N. Martín, *J. Mater. Chem.* **2008**, *18*, 1417 – 1426.

[5] J. L. Bahr, E. T. Mickelson, M. J. Bronikowski, R. E. Smalley, J. M. Tour, *Chem. Commun.* **2001**, 193 – 194.

[6] L. A. Girifalco, M. Hodak, R. S. Lee, *Phys. Rev. B* **2000**, *62*, 13104 – 13110.

[7] a) U. H. F. Bunz, S. Menning, N. Martín, *Angew. Chem.* **2012**, *124*, 7202 – 7209; *Angew. Chem. Int. Ed.* **2012**, *51*, 7094 – 7101; b) D. Tasis, N. Tagmatarchis, A. Bianco, M. Prato, *Chem. Rev.* **2006**, *106*, 1105 – 1136; c) G. Katsukis, C. Romero-Nieto, J. Malig, C. Ehli, D. M. Guldi, *Langmuir* **2012**, *28*, 11662; d) D. M. Guldi. V. Sgobba, *Chem. Commun.* **2011**, 606; e) G. Bottari, G. de la Torre, D. M. Guldi, T. Torres, *Chem. Rev.* **2010**, *110*, 6768.

[8] A. Hirsch, *Angew. Chem.* **2002**, *114*, 1933 – 1939; *Angew. Chem. Int. Ed.* **2002**, *41*, 1853 – 1859.

[9] Y. L. Zhao, J. F. Stoddart, *Acc. Chem. Res.* **2009**, *42*, 1161 – 1171.

[10] a) J. K. Sprafke, S. D. Stranks, J. H. Warner, R. J. Nicholas, H. L. Anderson, *Angew. Chem.* **2011**, *123*, 2361 – 2364; *Angew. Chem. Int. Ed.* **2011**, *50*, 2313 – 2316; b) H. Ozawa, X. Yi, T. Fujigaya, Y. Niidome, T. Asano, N. Nakashima, *J. Am. Chem. Soc.* **2011**, *133*, 14771 – 14777.

[11] G. R. Dieckmann, A. B. Dalton, P. A. Johnson, J. Razal, J. Chen, G. M. Giordano, E. Muñoz, I. H. Musselman, R. K. Draper, *J. Am. Chem. Soc.* **2003**, *125*, 1770 – 1777.

[12] M. Numata, M. Asai, K. Kaneko, A. H. Bae, T. Hasegawa, K. Sakurai, S. Shinkai, *J. Am. Chem. Soc.* **2005**, *127*, 5875 – 5884.

[13] H. Cathcart, V. Nicolosi, J. M. Hughes, W. J. Blau, J. M. Kelly, S. J. Quinn, J. N. Coleman, *J. Am. Chem. Soc.* **2008**, *130*, 12734 – 12744.

[14] a) Y. K. Kang, O. S. Lee, P. Deria, S. H. Kim, T. H. Park, D. A. Bonnell, J. G. Saven, M. J. Therien, *Nano Lett.* **2009**, *9*, 1414 – 1418; b) Z. Zhang, Y. Che, R. A. Smaldone, M. Xu, B. R. Bunes, J. S. Moore, L. Zang, *J. Am. Chem. Soc.* **2010**, *132*, 14113 – 14117; c) A. Llanes-Pallas, K. Yoosaf, H. Traboulsi, J. Mohanraj, T. Seldrum, J. Dumont, A. Minoia, R. Lazzaroni, N. Armaroli, D. Bonifazi, *J. Am. Chem. Soc.* **2011**, *133*, 15412 – 15424.

[15] J. L. López, C. Atienza, A. Insuasty, J. Lopez-Andarias, C. Romero-Nieto, D. M. Guldi, N. Martín, *Angew. Chem.* **2012**, *124*, 3923 – 3927; *Angew. Chem. Int. Ed.* **2012**, *51*, 3857 – 3861.

[16] C. Ehli, G. M. A. Rahman, N. Jux, D. Balbinot, D. M. Guldi, F. Paolucci, M. Marcaccio, D. Paolucci, M. Melle-Franco, F. Zerbetto, S. Campidelli, M. Prato, *J. Am. Chem. Soc.* **2006**, *128*, 11222 – 11231.

[17] a) H. J. Dai, *Acc. Chem. Res.* **2002**, *35*, 1035 – 1044; b) H. Hövel, M. Bodecker, B. Grimm, C. Rettig, *J. Appl. Phys.* **2002**, *92*, 771 – 777; c) G. S. Choi, Y. S. Cho, S. Y. Hong, J. b. Park, K. H. Son, D. J. Kim, *J. Appl. Phys.* **2002**, *91*, 3847 – 3854.

[18] a) R. Saito, T. Takeya, T. Kimura, G. Dresselhaus, M. S. Dresselhaus, *Phys. Rev. B* **1998**, *57*, 4145 – 4153; b) R. Saito, G. Dresselhaus, M. S. Dresselhaus, *Physical Properties of Carbon Nanotubes*, Imperial College Press, New York, **1998**.

[19] M. Zheng, A. Jagota, M. S. Strano, A. P. Santos, P. Barone, S. G. Chou, B. A. Diner, M. S. Dresselhaus, R. S. McLean, G. B. Onoa, G. G. Samsonidze, E. D. Semke, M. Usrey, D. J. Walls, *Science* **2003**, *302*, 1545 – 1548.

[20] M. A. Herranz, C. Ehli, S. Campidelli, M. Gutierrez, G. L. Hug, K. Ohkubo, S. Fukuzumi, M. Prato, N. Martin, D. M. Guldi, *J. Am. Chem. Soc.* **2008**, *130*, 66 – 73.

[21] C. Backes, C. D. Schmidt, F. Hauke, C. Boettcher, A. Hirsch, *J. Am. Chem. Soc.* **2009**, *131*, 2172 – 2184.

[22] **1** reveals upon 387 nm excitation a short lived transient—Figure S10.

